TOWARDS A KINETIC MODEL OF POTENTIAL-INDUCED SHUNTING

Christian Taubitz*, Matthias Schütze, Max B. Koentopp
Q-Cells SE, Sonnenallee 17-21, 06766 Bitterfeld-Wolfen, Germany
*corresponding author: c.taubitz@q-cells.com, +49-(0)3494-6699-52162

ABSTRACT: Potential-induced shunting (PIS) of wafer-based silicon solar cells is one of the most severe types of potential-induced degradation (PID). The correlation between laboratory PIS test results and the PIS behavior of PV modules in the field is still an open question. One reason for this is the fact that, due to intermittent stress, PIS is competing with regeneration episodes in the field unlike in most laboratory PIS setups. Since there is no detailed study of the regeneration from PIS available in literature, in this work, the overall kinetics of PIS is investigated. PIS is generated in the lab by applying a voltage bias to the cells of single-cell modules covered with grounded aluminum foil. Regeneration is enabled by eliminating voltage bias. The degradation and regeneration behavior is analyzed by shunt resistance (R_{sh}) measurements and performance measurements. It is found that in case of single-cell modules R_{sh} measurements are a suitable way to monitor the progress of PIS in terms of power degradation. The measurements reveal that the temperature dependences of both the shunting as well as the regeneration phase are Arrhenius like.
Keywords: lifetime, simulation, degradation, shunt, potential-induced

1 INTRODUCTION

In standard system architecture of photovoltaic (PV) installations solar cells incorporated in PV modules can be exposed to voltage bias of several hundred volts with respect to the module frames/mounting. This bias leads to leakage currents through the encapsulating material, which can cause various kinds of module damage. The degradation effects caused by such a voltage bias were named potential-induced degradation (PID) [1]. One of the most severe types of PID was discovered in the last few years and is affecting standard wafer-based p-type silicon solar cells under negative voltage bias. If certain conditions are met, this PID type can have a significant negative impact on the long-term performance of fielded modules by shunting of the solar cells [1-3]. In the following we will refer to this shunting PID as potential-induced shunting (PIS).

Numerous studies, e.g. [4] and references therein, showed that PIS is primarily connected with a fill-factor (*FF*) loss which is due to shunting of the cell's p/n-junction. The progression of PIS is associated with an increasing fraction of the cell being shunted and at the same time no longer contributing to short circuit current (I_{sc}) generation [5]. As a result of strong shunting, the open-circuit voltage V_{oc} is also reduced secondarily. PIS is commonly monitored by extracting *FF*, I_{sc}, and V_{oc} values from current-voltage (*I-V*) curves measured at standard test conditions (STC). The extent of shunting is usually evaluated from the slope of the *I-V* curve near I_{sc} ($V = 0$) assuming a constant (ohmic) shunt resistance $R_{sh} = dV / dI$. Nevertheless, in a recent study the correlation between the R_{sh} of sixty-cell modules and the corresponding performance loss was found to be poor [6]. Using two-diode model dark *I-V* curve fitting [7], it was revealed that the potential-induced shunt contains a significant nonlinear fraction [6]. In this work the correlation between PIS and the shunt resistance is studied in more detail in order to clarify this issue and to qualify this measurement for the investigation of PIS kinetics.

In spite of various PIS studies the correlation of PIS laboratory tests and PIS of modules under field conditions is still not well understood. In order to determine the acceleration introduced by certain lab conditions compared to the field, PIS caused in the laboratory can be compared to the PIS progress of identical fielded PV-modules [6][8]. Nevertheless, this approach is very time consuming and the obtained acceleration factors are only valid for the investigated test sites and module types. If the complete kinetics of PIS were known, such understanding could be used to develop a lifetime model, which can predict PIS levels from climate data for various regions.

Unfortunately there is only little information on the overall kinetics of PIS available in the literature. For PIS at continuous temperature-accelerated voltage-stress conditions an Arrhenius like behavior was found and an activation energy E_a of 0.726 ± 0.053 eV was estimated [6]. It is known that PIS regenerates if the voltage bias is removed and that this regeneration can be accelerated by temperature or reversed bias [1][5][9]. But no quantitative kinetics data is available for this regeneration so far. On the other hand, regeneration is a key parameter concerning PIS in the field. There are numerous and often extended episodes with no potential present at PV-modules' surfaces [8][10]. Moreover, module temperature is often high during these episodes (e.g. sunny days). Therefore as a main focus of this study the kinetics of both, PIS under negative voltage-bias conditions as well as the regeneration from PIS at zero voltage bias, are investigated. Regeneration under positive voltage-bias is not considered since it is not occurring under normal field conditions.

2 EXPERIMENTAL

In order to investigate the PIS kinetics, mini modules consisting of single p-type solar cells, specially engineered to be prone to PIS, were produced. These modules were PI-shunted in a climate chamber at different temperatures. Figure 1 shows the schematic of the experimental setup. The front glass of the single-cell module was covered with grounded aluminum foil and a high negative potential (-1 kV) was applied to the solar cell. In addition, on a regular basis the solar cell was biased with a voltage in reverse direction V_{rd} (< 0.3 V) and the dark current $I_d(V_{rd})$ was measured. This allowed for the determination of R_{sh} of the solar cell during the experiment assuming an ohmic shunt and correcting for

the serial resistance R_s introduced by the experimental setup which was determined separately:

$$R_{sh} = \frac{V_{rd}}{I_d(V_{rd})} - R_s \,. \qquad (1)$$

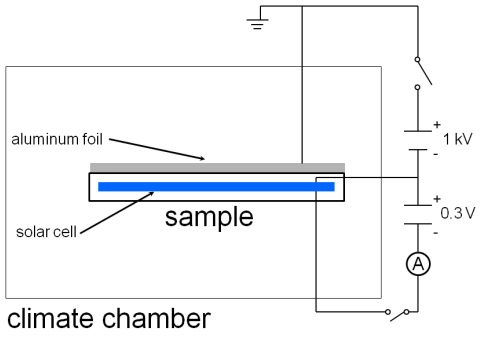

Figure 1: Schematic of the experimental setup for PIS and regeneration from PIS.

I-V curves at STC were measured to investigate the impact of PIS on the sample performance. For this purpose, the degradation/regeneration processes had to be interrupted and the samples had to be cooled down. Special care was taken to minimize the time needed for this interruption in order to avoid regeneration at conditions not well defined. Unintended regeneration was checked for by measuring R_{sh} before and after the interruptions. Measurements were rejected if the relative change in R_{sh} was bigger than 30%. For all valid measurements the mean of R_{sh} measured before and after the interruption was used.

3 RESULTS AND DISCUSSION

3.1 Measurement of PIS

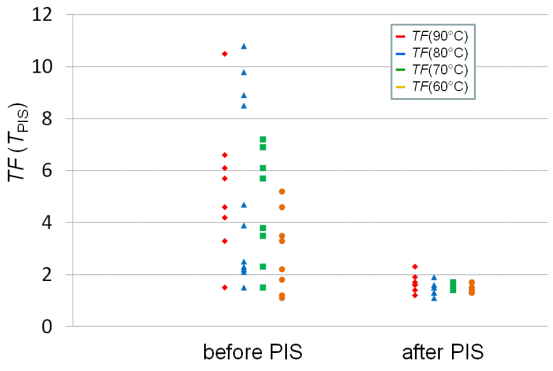

Figure 2: R_{sh} temperature factors ($TF(T_{PIS})$) for single-cell modules before and after PIS at different temperatures.

The R_{sh} of solar cells can be temperature dependent. The correlation between R_{sh} measured at the elevated temperature during PIS/regeneration (T_{PIS}) and R_{sh} measured at room temperature (RT) was determined in a first step. Figure 2 shows values of the temperature factor $TF(T_{PIS})$ = R_{sh}(RT) / $R_{sh}(T_{PIS})$ for several single-cell modules. *TF* was determined before PIS (R_{sh} >> 10^5 Ωcm^2) and after PIS ($R_{sh} \leq 10^5$ Ωcm^2). *TF* values before PIS cover a wide range for different single-cell modules with most of the samples showing high *TF* > 2. In contrast, after PIS all modules show quite similar *TF*, mostly < 2.

This R_{sh} behavior-change indicates that the dominant shunting mechanism changes with the progression of PIS. Before PIS intrinsic shunts determine the R_{sh} of the solar cell ($R_{sh,int}$). These shunts can have a variety of different origins, e.g. incomplete edge isolation. This variety could explain the wide range of *TF*. With the onset of PIS a second shunting mechanism appears ($R_{sh,PIS}$), which soon becomes dominant and therefore determines the temperature behavior. This mechanism shows a low *TF*. Both R_{sh}-types can be regarded as electrically connected in parallel. Thus, $R_{sh,PIS}$ can be calculated from the R_{sh} measured according to (1) ($R_{sh,meas}$) by

$$R_{sh,PIS} = \left(\left(R_{sh,meas}\right)^{-1} - \left(R_{sh,int}\right)^{-1}\right)^{-1} . \qquad (2)$$

Note that this relation is only valid for a certain, fixed temperature. If $R_{sh,meas}$ and $R_{sh,int}$ are measured at the same temperature T_{PIS}, $R_{sh,PIS}$ is given by (2) at T_{PIS} too. The determined $TF(T_{PIS})$ was used to calculate $R_{sh,PIS}$(RT) from $R_{sh,PIS}(T_{PIS})$ if necessary.

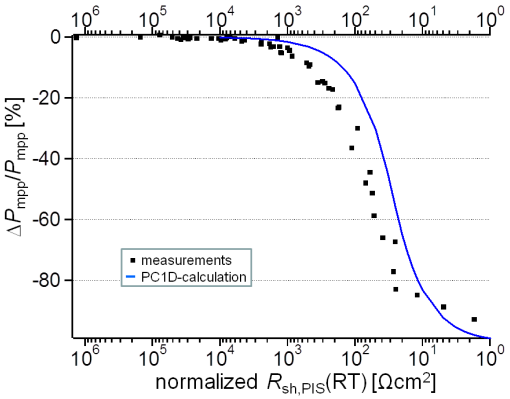

Figure 3: Measured relative loss of P_{mpp} versus $R_{sh,PIS}$(RT) normalized to the cell area for single-cell modules. The blue line represents model calculations assuming ohmic shunting only.

The values of $R_{sh,PIS}$(RT) determined this way were compared to the measured loss of power ΔP_{mpp} at the maximum-power point of the *I-V* curve. The results for single–cell modules are shown in Fig. 3 (symbols). The power loss calculated with the numerical device simulator PC1D [11] for varying R_{sh} is given for comparison (solid line). There is a strong correlation between $R_{sh,PIS}$(RT) and $\Delta P_{mpp}/P_{mpp}$. The correlation is in good agreement with the PC1D simulation except for a nearly constant shift along the logarithmic R_{sh} scale.

The reason for this shift becomes apparent by comparing a measured PIS affected *I-V* curve with one calculated using a two-diode model [6] assuming only a reduction in the ohmic shunt resistance due to PIS equal to the measured $R_{sh,PIS}$, see Fig. 4. The slopes of the measured curves (symbols) for negative voltages are represented well by the model (blue and green line).

Nevertheless, there is an increasing gap with increasing positive voltage between the measured curve after PIS and the model curve. This shows that the assumption of ohmic behavior of the PIS-shunt introduces some error. Modelling of the nonlinear shunt with a second diode with ideality factor n_2 yields much better agreement (red line in Fig. 4).

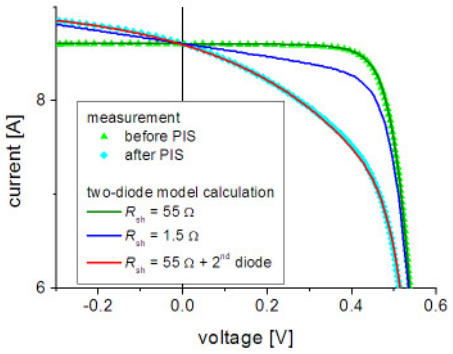

Figure 4: Comparison of *I-V* curves before and after PIS with simulated curves assuming ohmic shunt behavior only (green and blue line) or with nonlinear shunting (red line).

It was found that not only the shunt current increases with progressing PIS but also n_2 needs to be changed in order to achieve a best fit of the model to the measured *I-V* curves. This is in agreement with the findings of a recent study [6]. n_2-values larger than 10 were determined in the present study for strong PIS with $\Delta P_{mpp}/P_{mpp} > 10\%$. Note, that an increasing n_2 results in decreasing nonlinearity of the shunt for a given voltage range. Thus, the error introduced by the assumption of a linear shunt is reduced with progression of PIS. This can be seen tentatively in Fig. 3 by a decreasing gap between measurement and the PC1D-simulation.

Although the assumption of a linear behavior of the PIS shunt is insufficient for accurate determination of the associated power loss, there is an unambiguous relation between $R_{sh,PIS}$(RT) and $\Delta P_{mpp}/P_{mpp}$. This relation allows for an estimation of the unknown ΔP_{mpp} due to PIS via the measurement of $R_{sh,PIS}$(RT) which is convenient and easy to implement. Thus, the measurement of $R_{sh,PIS}$(RT) can be used to monitor the progress of PIS of single-cell modules. This finding seems to be in conflict with the results of a recent study [6]. But in contrast to the present study, the authors investigated 60-cell module instead of single-cell modules. In order to check weather this is the reason for the apparent discrepancy, the comparison of $R_{sh,PIS}$(RT) and $\Delta P_{mpp}/P_{mpp}$ was also done for 60-cell modules here. Note that in contrast to the single-cell modules, where the R_{sh} was determined in reverse direction (see section 2), the R_{sh} was determined for 60-cell modules from I_d measured at forward bias < 6 V, because the by-pass diodes could not be removed for every module. Results shown in Fig. 5 exhibit the same poor correlation that was reported before [6]. The serial interconnection of multiple cells likely in conjunction with different degrees of PIS of the individual cells leads to worse applicability of the simple assumption of ohmic shunting.

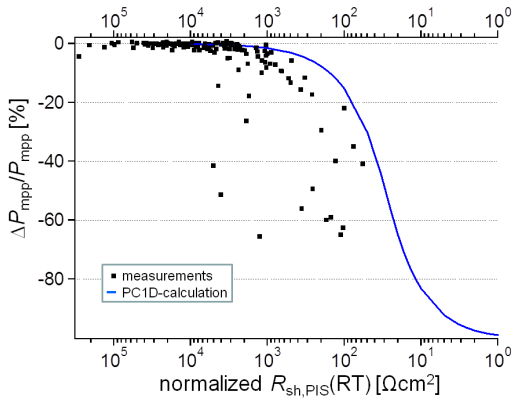

Figure 5: Measured relative loss of P_{mpp} versus $R_{sh,PIS}$(RT) per cell normalized to the area of one cell for 60-cell modules. The blue line represents model calculations assuming ohmic shunting only.

3.2 PIS kinetics

Figure 6 shows the $R_{sh,PIS}$-measurement of a single-cell module that was PI-shunted applying a voltage bias of -1 kV for about 9 minutes at 90°C. Consecutively the voltage bias was set to zero simulating a dry glass surface or nighttime conditions. The $R_{sh,PIS}$-behavior can be separated into three distinct phases.

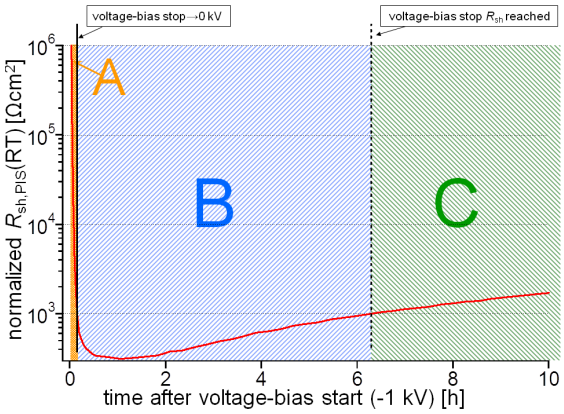

Figure 6: $R_{sh,PIS}$-measurement of a single-cell module during and after PIS at 90°C. The $R_{sh,PIS}$-behavior can be separated into 3 distinct phases: shunting (A), transition phase (B) and regeneration (C).

At first, due to the voltage bias, PIS takes place, which leads to a rapid decrease of the $R_{sh,PIS}$-value (phase A).

When the $R_{sh,PIS}$-value normalized to the cell area dropped to some kΩcm², the voltage bias was set to zero by disconnecting the voltage source and shorting the solar cell to the aluminum covered glass surface. Surprisingly the decrease of the $R_{sh,PIS}$ does not stop immediately. In this transition phase B, the shunting of the solar cell goes on for about 1 hour although slowing down gradually. Finally the degradation stops and the $R_{sh,PIS}$-value slowly starts to increase again. Two different mechanisms seem to compete in this phase, one leading to further shunting of the cell, the other recovering $R_{sh,PIS}$.

In the third phase C of the PIS kinetics only regeneration from PIS takes place as visible by a continuous increase of the $R_{sh,PIS}$-value. Here the shunting mechanism appears to have mostly vanished. The

transition between phase B and C was defined as the time when the $R_{sh,PIS}$ value measured at voltage-bias stop was regained by the ascending curve (vertical dashed line in Fig. 6). It can be seen that the regeneration in phase C is much slower than PIS in phase A.

Six single-cell modules were PI-shunted at 90°C, 80°C, 70°C, and 60°C, respectively, and regenerated afterwards without temperature change just by eliminating voltage-bias resulting in $R_{sh,PIS}$ curves similar to the one shown in Fig. 6. The time with applied voltage bias (phase A) was identical for all modules degraded at the same temperature and chosen in order to reach a comparable R_{sh}-level for all temperatures. In the following sections the $R_{sh,PIS}$-measurements are used to investigate the three phases A-C of PIS kinetics in more detail.

3.2.1 Shunting phase A

Figure 7 shows the $R_{sh,PIS}$-measurement of all 24 single-cell modules during PIS in phase A. The time axis was set to zero at the start of voltage bias (-1 kV). The time of voltage-bias stop is depicted by vertical lines for each temperature group. In order to analyze the temperature dependence of PIS, the time in which the $R_{sh,PIS}$ decreases to a constant target value (dashed line in Fig. 7) is compared.

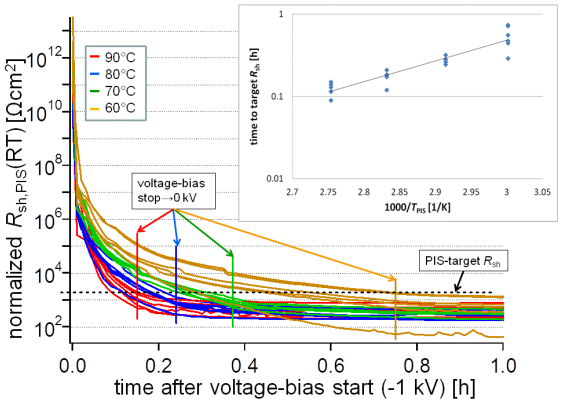

Figure 7: $R_{sh,PIS}$-measurement of single-cell modules during PIS at different temperatures. The voltage bias stop and the PIS target value are depicted by vertical and horizontal lines, respectively. In the inset an Arrhenius plot of the time to reach the PIS target value is shown.

Although there is quite a big difference between the PIS behavior of individual modules at the same temperature, it can be seen that a decrease of the module temperature leads to a slowing down of PIS. In the inset of Fig. 7 an Arrhenius plot of the time to reach the $R_{sh,PIS}$ target value is shown. The straight line represents the best fit to the data which is described by an E_a of approximately 0.5 eV. Due to the already mentioned big difference in PIS behavior the scattering of the points in the Arrhenius plot introduce a large error in E_a which is estimated to be at least 0.2 eV. Taking into account this uncertainty, this value is in agreement with the literature [6].

3.2.2 Transition phase B

As already shown in section 3.2, a vanishing potential does not lead to an immediate stop of PIS. For a certain time the decrease of the $R_{sh,PIS}$ goes on although gradually slowing down. Finally the decrease stops and $R_{sh,PIS}$ starts to increase. Figure 8 shows the $R_{sh,PIS}$-measurement of one representative single-cell module at 90°C, 80°C, 70°C, and 60°C, respectively, directly after voltage-bias stop. The measurements are normalized to the minimum $R_{sh,PIS}$ for easier comparison. A temperature dependence of the $R_{sh,PIS}$-behavior in the transition phase becomes apparent. A lowering of temperature leads to

a) a slowdown of the $R_{sh,PIS}$ decay,
b) an increase of the time until the $R_{sh,PIS}$-value reaches its minimum, and
c) a slowdown of the $R_{sh,PIS}$ increase after reaching its minimum.

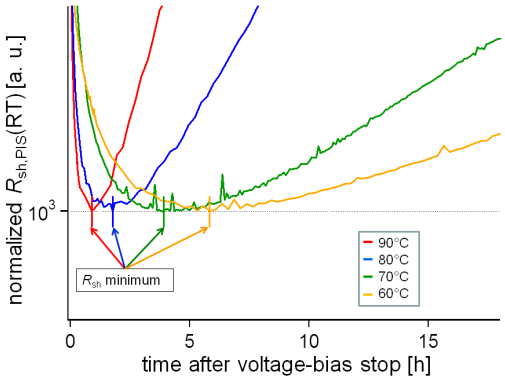

Figure 8: $R_{sh,PIS}$-measurement of single-cell modules directly after PIS at different temperatures. The $R_{sh,PIS}$-measurements are normalized to the curve minima which are depicted by vertical lines.

As mentioned before, in the transition phase two competing mechanisms seem to exist. The temperature dependence of the $R_{sh,PIS}$-behavior can be explained by simultaneous slowdown of both mechanisms with decreasing temperature.

3.2.3 Regeneration phase C

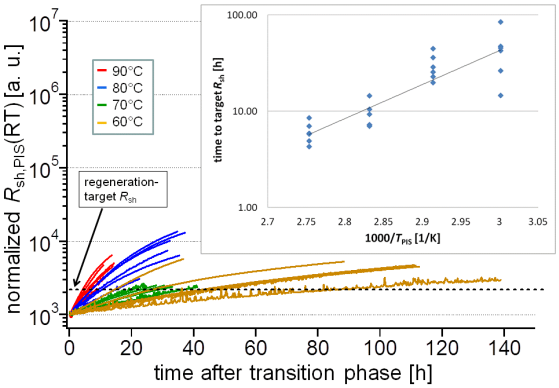

Figure 9: $R_{sh,PIS}$-measurement of single-cell modules at different temperatures and zero voltage bias after PIS. The regeneration target value is depicted by a dashed horizontal line. In the inset an Arrhenius plot of the time to reach the regeneration target value is shown.

Figure 9 shows the $R_{sh,PIS}$-measurement of all modules after $R_{sh,PIS}$ recovered to the value at voltage-bias stop (phase C). The time at which the value at voltage-bias stop was recovered was set to zero and the curves were normalized to the $R_{sh,PIS}$-value at that time for comparison. The regeneration from PIS in this phase

C appears to be much slower than degradation in phase A for all samples (note the different timescale). The difference might be due to the missing driving force represented by a voltage bias which is present for the degradation only.

In order to analyze the temperature dependence of regeneration, the times required for increasing $R_{sh,PIS}$ by a factor of 2.2, i.e. to reach the target value depicted by the dashed line in Fig. 9, are compared. The regeneration behavior of individual modules at the same temperature varies quite a lot similar to the PIS behavior in phase A. Nevertheless, a pronounced temperature dependence of regeneration from PIS becomes apparent. An Arrhenius plot of the time to reach the regeneration target value is shown in the inset of Fig. 9. The straight line represents the best fit to the data using an E_a of about 0.7 eV. Again, due to the strong variations within the temperature groups, there is a big uncertainty which is estimated to be at least 0.3 eV. Within that limit this E_a for regeneration is not significantly different from the one obtained before for PIS. This finding is consistent with the hypothesis that the transport of the same thermally activated species is responsible for PIS as well as for the regeneration from PIS.

4 SUMMARY

In this work, the overall PIS kinetics was investigated in order to make first steps towards a PIS lifetime model. The PIS progress of single-cell modules was monitored using the apparent linear shunt resistance R_{sh} calculated from the measured dark current at reverse bias, which was found to be an appropriate way to monitor PIS progression, in spite of a nonlinear shunt contribution. The temperature dependence of R_{sh} before and after PIS revealed that due to PIS an additional shunting mechanism appears beside intrinsic shunts and becomes dominant.

Single-cell modules that were PI-shunted at different temperatures were regenerated at the same temperatures by eliminating the voltage bias. It was found that the degradation did not stop immediately after voltage-bias stop. The time after voltage-bias stop to reach the minimum R_{sh} was found to be temperature dependent. It was shown that PIS under voltage bias as well as the regeneration from PIS without voltage bias can be modeled by an Arrhenius-like temperature behavior. Activation energies of 0.5 ± 0.2 eV and 0.7 ± 0.3 eV respectively were estimated. This is in agreement with the hypothesis that the transport of the same temperature activated species is responsible for PIS under voltage bias and the regeneration from PIS without voltage bias. It was found that for every temperature the regeneration from PIS without voltage bias is much slower than the degradation at -1 kV.

4 ACKNOWLEDGEMENT

The authors gratefully acknowledge the financial support by the German Federal Ministry of Education and Research within the framework of the Leading-Edge Cluster Competition and Solarvalley Central Germany under contract No03SF0399I. The authors also gratefully acknowledge Ruth Konieczny for the assistance with the experiments.

6 REFERENCES

[1] S. Pingel et al., 35th IEEE Photovoltaic Specialists Conference, 2010, Hawaii .
[2] P. Hacke et al., 35th IEEE Photovoltaic Specialists Conference, 2010, Hawaii.
[3] P. Hacke et al., 25th European Photovoltaic Solar Energy Conference, 2010, Valencia.
[4] H. Nagel et al., 26th European Photovoltaic Solar Energy Conference, 2011, Hamburg.
[5] M. Schütze et al., 37th IEEE Photovoltaic Specialists Conference , 2011, Seattle.
[6] P. Hacke et al., 38th IEEE Photovoltaic Specialists Conference, 2012, Austin.
[7] D.L. King et al, 26th IEEE Photovoltaic Specialists Conference, 1997, Anaheim.
[8] S. Hoffmann et al., Prog. Photovolt: Res. Appl., 2012, DOI: 10.1002/pip.2238.
[9] P. Hacke et al., 37th IEEE Photovoltaic Specialists Conference, 2011, Seattle.
[10] M. Schütze et al., 26th European Photovoltaic Solar Energy Conference, 2011, Hamburg.
[11] P. Basore, IEEE Trans. Electron Devices, 37 (2), 1990, pp. 337–343.